Published by: ***Higher Institute of Engineering and Technology, Kafrelsheikh.*** **(KFS-H.I.E.T)**

Journal homepage: https://jiet.journals.ekb.eg/

Print ISSN 3009-7207 **Online ISSN** 3009-7568

FE Simulations of Ferrocement Box Columns Filled with Lightweight Concrete

Yousry B. Shaheen[1], Boshra A. Eltaly[1], *Ahmed T. EL-boridy[2]

[1]*Civil Engineering Department, Menoufia University, Shebin El Koum, Egypt*

[2]*Civil Engineering Department, Higher Institute of Engineering and Technology, Kafrelsheikh, Egypt*

Received: 5 April 2024; Revised: 10 July 2024; Accepted: 13 July 2024

ABSTRACT: The Finite Element Method (FEM) has expanded in usage and popularity in recent years. It is now one of the fundamental techniques for analyzing how elements of reinforced structures behave. Because of its benefits over the majority of other numerical approaches, the Finite Element Analysis (FEA) method has proven to be a particularly strong tool in engineering analysis. The purpose of the research is to compare the practical results experimental studied and the theoretical results from the ANSES program. This study examined the behavior of columns until failure using the ANSYS 19 program and the finite element approach. To lower the column's weight and, consequently, the loads on the soil during foundation design, this research aims to create lightweight concrete box columns using various base materials at a lower cost. The ANSYS 19 program is used to explore finite element (FE) modelling. Eleven square short column specimens with side lengths of 200 mm, heights of 1000 mm, and basic box dimensions of 100 × 100 mm along the height of the column were modelled for this study. Axial and eccentric loads were applied to the samples until collapse happened. Previous research's experimental results were used to validate the finite element models used in this investigation. The ratio between the vertical displacements of the experimental and analytical findings ranged from 5.1% to 19.34%, and the ratio between the experimental and analytical ultimate loads ranged from 0.68 to 4.19%. The horizontality of the experimental and analytical results ranged from 3.83% to 21.27% in the displacement ratio.

KEYWORDS: Ferrocement concrete, lightweight concrete, finite element analysis, ANSYS 19, box columns, displacement, eccentricity.

1. INTRODUCTION

Nowadays, a lot of Portland cement is used in buildings. Tests for fracture control, impact resistance, and durability have shown that the material performs remarkably well because of the close spacing and homogenous distribution of reinforcement fibers within it. Ferrocement, often known as thin-wall reinforced concrete, is normally strengthened with thin, independently built layers of continuous wire mesh using hydraulic cement mortar. A wide range of objects, such as tanks, precast concrete components, roofs, retaining walls, bridge decks, sculptures, restoration projects, and other roof systems, are built using Portland cement [1–8].

Conventional reinforced concrete (RC). in fact, reinforced concrete is considered as a composite can be produced in any new shape because no coarse material is used, and the mesh can be correctly rolled and connected to the structural bar. A variety of test results can also be used to create quality standards for the construction and maintenance of structural parts [9–12].

Ferrocement has a high surface area and relatively strong bonding forces between the mesh and cement slurry since it lacks typical reinforced steel bars and coarse aggregate, allowing it to be shaped into any shape [13, 14]. Many studies use mesh contrast modification to enhance the ferrocement mortar's characteristics [15–18]. The closely spaced wire mesh increases the ductility of the ferrocement composite.

Prior studies looked at the effects of making dense mortar with fly ash and silica fume. Steel wire mesh was substituted for galvanized wire mesh. Although this increased the bearing capacity of the ferrocement compounds, it eventually lost its effectiveness and caused the compounds' performance attributes to decline. The benefits of reinforcing ferrocement concrete using polypropylene fibers include decreased corrosion, avoided structural damage, and increased concrete life [19, 20].

 *Corresponding author email: ahmedelboridy1993@gmail.com

The structural components of various reinforced concrete members, such as panels, beams, or columns, are strengthened and restored with the application of ferrocement. In their investigation into the impact of polypropylene (PP) fibers on the behavior of FC slabs, [21] found that PP fibers increased the number of cracks and the slab's load capacity. [22] investigation of the behavior of FC slabs using layers of wire mesh was a creative way to increase the slab capacity and a novel way to improve the strength of the beam which means the resistance of the beams to the stresses generated as a result of shearing and bending, which has been applied in numerous earlier studies to reinforce, restore, and repair traditional RC beams [23–27].

Columns, one of the most crucial structural components of reinforced concrete structures, have the power to influence the behavior and mode of failure of the structure. Over the past few decades, RC structures have broken numerous times due to excessive service loads, durability issues, and seismic stresses. Under axial and eccentric compression, [28] conducted an experimental study on short box-section ferrocement columns with and without concrete grout. Based on an analysis of the types, configurations, and size ratios of reinforcement, as well as test results, it was shown that welded wire mesh performs better than woven mesh of the same size. The reinforced column has a significantly higher strength and ductility than the reference column without reinforcement, according to [29] study of RC columns with longitudinal steel and ferrocement under static axial stress. [30] conducted an experimental study with varying volumetric ratios of ties to examine the impact of lateral reinforcement of short square reinforced concrete columns employing a single a layer expanded metal mesh (EMM). The strength and ductility of the current columns were found to have significantly improved as a result of the suggested lateral reinforcement. Furthermore, without lowering the final load, a considerable decrease in the volumetric ratio of the ties can be accomplished by using an Expanded wire mesh (EMM) layer. It is possible to create new reinforced concrete columns with high strength, resistance to cracking, and high ductility properties by using advanced composite materials, according to [31] study of the structural behavior of reinforced composite concrete columns with varying proportions of different types of metal and non-metallic mesh reinforcement. Furthermore, an experimental program was conducted by [32] to study the behavior of lightweight hollow ferrocement blocks that are used to reinforce lightweight ferrocement columns. Based on the test results, improvements were found in terms of crack resistance, serviceability, ultimate loads, and good compatibility. In order to show how these circular hollow concrete columns react to eccentric and concentric axial compressive forces, [33] cast and tested eight columns. They found that for columns strengthened with a single layer of welded wire mesh (WWM), the change from concentric to eccentric force reduced the ultimate load value by 73.5%.

The behavior of reinforcing columns with steel mesh layers and ferrocement concrete has been extensively researched in the past [34–41], and it has been shown to be a creative technique for increasing column capacity. Furthermore, the impact of strengthening short columns with ferrocement jackets was investigated by [42]. It was shown that using ferrocement as a reinforcement method raised the average strength of columns from 11% to 40%. [43] investigated the strength and behavior of RC columns reinforced with ferrocement jackets. Extensive external restraints along the length of RC columns greatly boost their ductility, according to test data. In comparison to the control column, the axial load capacity and axial stiffness of RC square columns jacketed with this kind of ferrocement concrete rose by roughly 33% and 26%, respectively, according to [44]. According to test results, ferrocement jacketing raises the ultimate axial deflection of the RC column and enhances its capacity to improve the ultimate load. [45] examined the ferrocement jacket reinforcing of square RC columns under compressive load.

Using the ANSYS software, researchers have investigated the use of the finite element method to predict structural element behavior. Previous research has demonstrated that by quickly anticipating the structural behavior, the finite element method (FEM) with ANSYS can save time and money [46–56]. According to the literature, not much research has been done on hollow ferrocement columns, especially ones that contain steel meshes serving as lateral reinforcement instead of traditional stirrups. Furthermore, no previous studies on lightweight material hollow-core FC columns have been conducted. Thus, this study examined how lightweight ferrocement composite box columns behaved under eccentric and concentric loads. This study looked at the hollow core filled with lightweight concrete ferrocement composite columns that have been tested before in the literature [7]. Additionally, the primary goal of this work was to use ANSYS 19 to investigate the overall structural performance and efficiency of hollow ferrocement columns with box apertures. The behavior of every tested each column simulated and examined using this finite element analysis program, which makes use of finite element method and can offer a trustworthy way to numerically forecast experimental outcomes.

2. GEOMETRIC DIMENSIONS OF COLUMNS

Eleven square columns measuring 200 × 200 mm, column height 1000 mm, and box core dimensions 100 × 100 mm along the column height were studied. The specimens underwent axial and eccentric load testing up until the point of failure. Additionally, research the effects of various characteristics like ductility, energy absorption, hardness, strength, and cracking behavior. Since a major reinforcement of 4 Ø 10 was utilized for all samples and Ø6 stirrups, the

reinforcement ratio, sample dimensions, and blank dimensions were set. Every sample was made using the same kind of wire mesh. This kind of mesh is made of welded wire, and each sample had the same number of layers. To compare solid, hollow, Hollow columns filled with these materials columns under axial and eccentric stresses, various materials were placed inside the core. These materials included lightweight concrete and lightweight bricks. The test results and conclusions, as well as the prior study [7]. Table 1 displays the geometric dimensions of the columns that were simulated in this study using the FEM. The columns' specifics are displayed in Figure 1. The columns were cast and tested in the prior research [7].

Table 1: Tested column details [7]

Column	Concrete type	welded wire mesh (WWM)	Lateral stirrups	Load condition	Holing condition	Filling material
A1	NWC	NA	Ø6@150mm	Axial load	without	NWC
A2					with	Empty
B1	FC	Two layers	NA		with	Empty
B2					with	BLWC
B3					with	FLWC
B4					with	Brick
C1	NWC	NA	Ø6@150mm	Eccentric load (e = 0.2 B)	without	NWC
C2					with	Empty
D1	FC	Two layers	NA		with	BLWC
D2					with	FLWC
D3					with	Brick

Where, FC is Ferrocement Concrete, NWC is normal Weight Concrete, BLWC is brick Lightweight Concrete, FLWC is foam Lightweight Concrete, Brick is lightweight bricks, NA is unavailable.

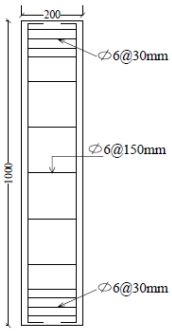

(a) Longitudinal section of NWC columns

(b) Elevation view of FC columns

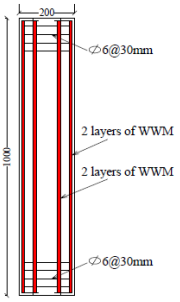

(c) Longitudinal section of FC columns

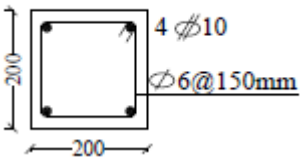

(d) A1 and C1 section

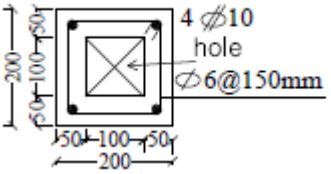

(e) A2 and C2 section

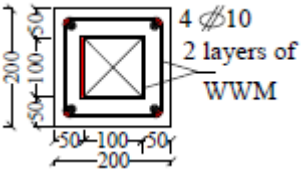

(f) B1 section

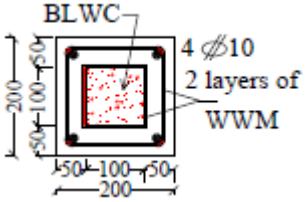

(g) B2 and D1 section

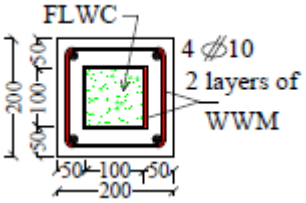

(h) B3 and D2 section

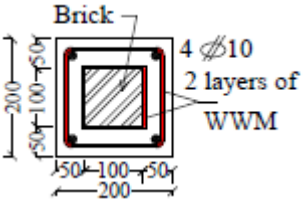

(i) B4 and D3 section

Fig.1. Details of the Tested Columns

3. PROPERTIES OF THE MATERIALS USED

The mixing ratios employed in earlier studies are displayed in Tables 2–5 [7]. The NWC mixture proportions are shown in Table 2, and after 28 days, the NWC had tensile and compressive strengths of 2.5 and 25.5 MPa, respectively. The amounts of the concrete mortar (FC) combination are listed in Table 3. After 28 days, the FC achieved 3.5 MPa for splitting tensile strength and 36 MPa for compressive strength. The BLWC mixture's proportions are displayed in Table 4. The BLWC mixture reached compressive and tensile strengths of 11 MPa and 1.2 MPa after 28 days. Table 5 lists each proportion of the FLWC mix. The FLWC mix achieved compressive and tensile strengths of 5 MPa and 0.45 MPa after 28 days. The ANSYS program was used to enter these values. The load-axial displacement relationships for the columns, taking into account the experimental and FE responses, are depicted in Figs. 8.

Table 2: Compositions of NWC Mixture [7]

Component	Water	Coarse aggregate	Fine aggregate	Portland cement
Quantity (kg/m3)	130	1330	665	350

Table 3: Proportions of FC Mix [7]

Component	PP Fiber	Fine aggregate	Water	fly ash	Silica fume	Portland cement	Superplasticizers
Quantity (kg/m3)	1.2	1200	275	120	45	450	12.2

Table 4: Proportions of BLWC Mix [7]

Component	Fine aggregate	Silica fume	Portland cement	PP Fiber	LAABA	Superplasticize	Water
Amount (kg/m3)	**701**	**45**	**405**	**1.2**	**420**	**9**	**171**

Table 5: Proportions of FLWC Mixture [7]

Component	Superplasticizer	Water	Silica fume	EP aggregate	Fine aggregate	Portland cement
Amount (kg/m3)	**6.75**	**205**	**45**	**23.5**	**500**	**450**

4. TEST SETUP AND MEASUREMENTS

Figure 2 depicts the test configuration and instruments used in earlier studies [7]. The load on top of the tested column was provided by a 3000 kN hydraulic jack. Robust steel caps are affixed at both extremities of the column to avert localised failure of the concrete crushing and to effectively disperse the imposed weight.

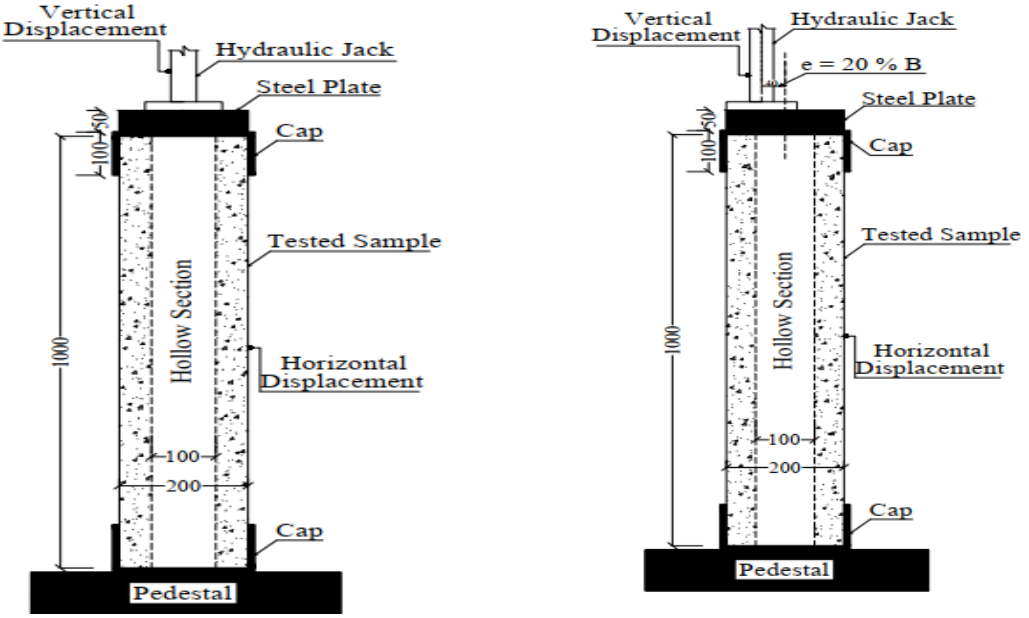

(a) central load **(b) eccentric load.**

Fig.2. Test setup and measurements for the columns, Dim. in mm [7]

To record the load, a load cell is connected to the socket. The vertical displacement of the column (shortening) was measured with a displacement transducer (DT1). The mid-shaft's horizontal displacement was also recorded using DT2. On the sides of each column are markings indicative of the crack patterns.

5. FINITE ELEMENT MODEL USING ANSYS

The use and acceptance of the Finite Element Method (FEM) have grown recently. These days, it's one of the most important methods for assessing how members of reinforced structures behave. The Finite Element Analysis (FEA) method has proven to be a very powerful tool in engineering analysis due to its advantages over most other numerical approaches. The development of the Finite Element Method (FEM) and the growing usage of computers have made it feasible to conduct realistic analyses of more complex systems. The more intricate the structural engineering layout of large structural structures, the greater the need for computer-based numerical solutions. However, experimental studies might be impractical at times and need a significant investment of time, money, and effort. In this study, the behavior of columns until failure was examined using the finite element method with the ANSYS 19 program. The outcomes of the tests were compared with the theoretical models that were generated. Steel reinforcement in finite elements was modelled using the element (LINK8) and the reinforced mortar layers were modelled using the element (SOLID65) [52].

Because the columns in the current investigation were loaded to the point of failure, nonlinear material analysis (plasticity) and cracking were employed. The program requires input for the modulus of elasticity, Poisson's ratio, and the relationship between stress and strain in order to model the plasticity of mortar. As seen in Figure 3, the column with its dimensions was initially constructed as a volume and later defined as a Solid65 element. The concrete mixture with Fcu = 36, 25.5, 11, 5 MPa for FC, NWC, BLWC, and FLWC, respectively, was modelled using this element. It was expected that the tensile strength of concrete (Fctr) would be identical to the value found in Equation 1 [57], where Fctr for FC, NWC, BLWC, and FLWC, respectively, would be 4, 3.2, 2, and 1.4 MPa. An opening crack's (C1) shear transfer coefficient was calculated to be 0.8. The closed fracture (C2) was assumed to have a shear transfer coefficient of 1.

$$f_{ctr} = 0.6\sqrt{f_{cu}} \tag{1}$$

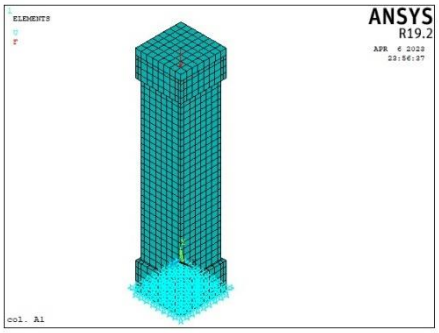

Fig.3. The studied column as solid 65 elements

By taking into account the compressive strength of concrete at 28 days (Fcu), which is equal to 36, 25.5, 11, and 5 MPa for FC, NWC, BLWC, and FLWC, respectively, and the weight (Wc) of FLWC, BLWC, NWC, and FC, which is 1060, 1770, 2500, and 2300 kg/m³, respectively, one can calculate the modulus of elasticity of used mortar (Ec) using Equation 2 in accordance with AISC 360-10 (AISC 2010) [57]. Equation 3 can be used to calculate the multi-linear isotropic stress-strain curve for the concrete. In this analysis, Poisson's ratio for four mortars is 0.2.

$$Ec = 0.043 W_c^{1.5} \sqrt{f_c'} \tag{2}$$

$$f = \frac{E_c\, \varepsilon}{1+(\varepsilon/\varepsilon_o)^2} \tag{3}$$

Where Wc is the weight of concrete per unit volume, F is stress at any strain (ε), and $\varepsilon_\circ$ is the strain at the ultimate compressive strength at 28 days, which can be calculated from Equation 4. $F_{c\backslash}$ is the cylindrical compressive strength of the concrete ($F_{c\backslash} = F_{cu}$ /1.25). The stress-strain curve was computed using these equations and is displayed in Figure 4-7.

$$\varepsilon_\circ = \frac{2F_{cu}}{E_c} \tag{4}$$

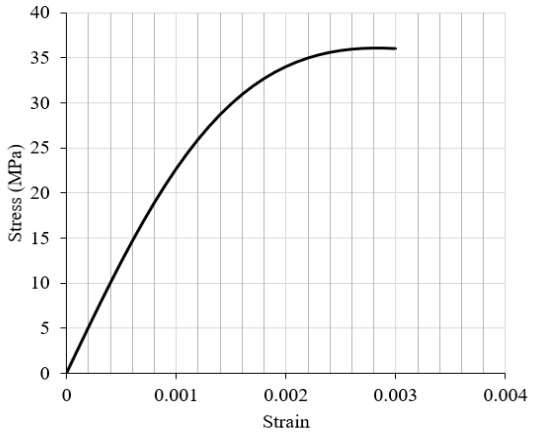

Fig.4. Stress-strain curve of FC [7].

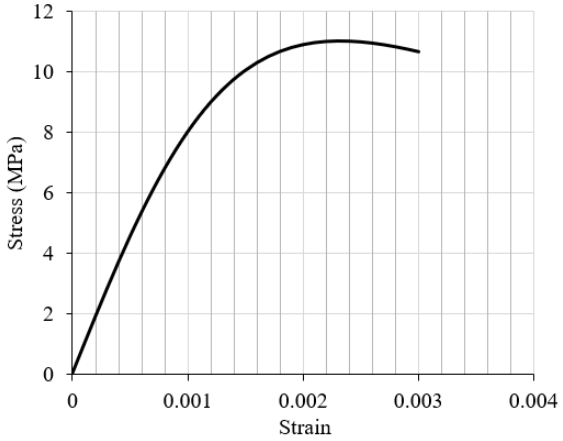

Fig.5. Stress-strain curve of BLWC [7].

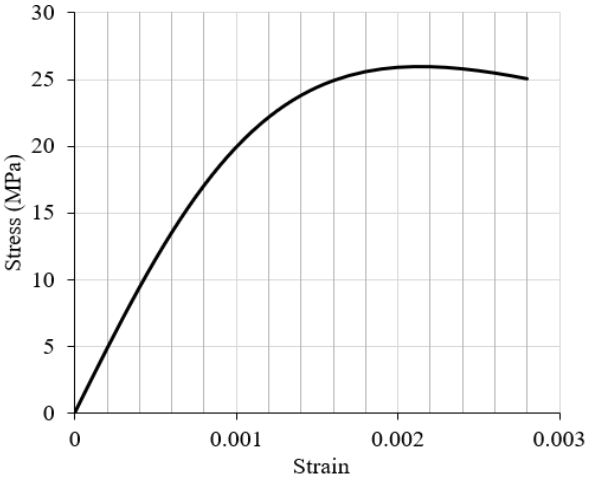

Fig.6. Stress-strain curve of NWC [7].

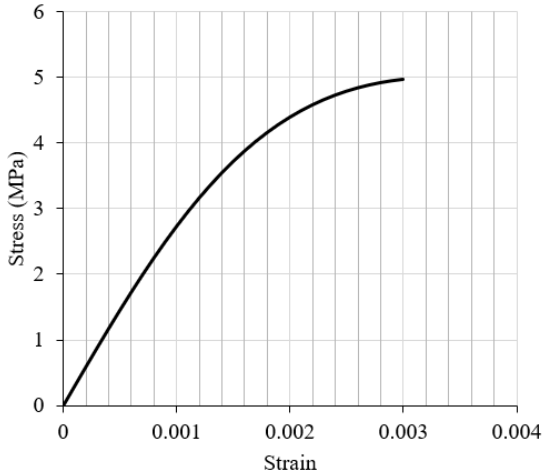

Fig.7. Stress-strain curve of FLWC [7].

The real stress-strain curve from tensile tests served as the basis for the steel reinforcement stress-strain curve in the finite element model. However, the negative slope component of the stress-strain curve was removed in order to increase the convergence of the finite element model. After yielding, the zero-slope section was also somewhat altered to have a mildly positive slope. As shown in Figure 8, the ordinary mild steel was modelled using link spar 8 components, giving rise to cross-section areas of 28.27 mm^2 for stirrup steel with a 6 mm diameter and 78.54 mm^2 for the upper steel with a 10 mm diameter.

The following are the material properties for the steel reinforcement model: In this analysis, the elastic modulus is Es = 200 GPa, the yield stress for stirrups steel is fy = 240 MPa, the yield stress for upper and lower steel is fy = 360 MPa, and Poisson's ratio is 0.3.

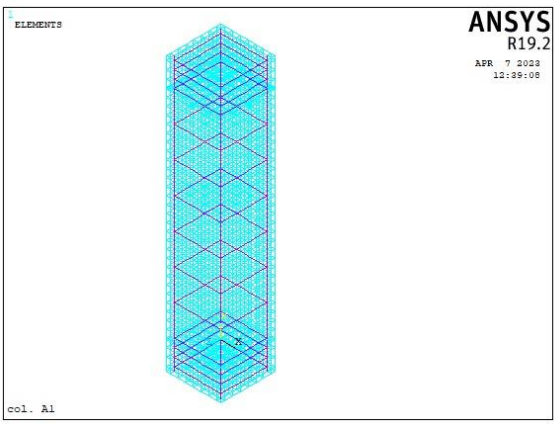

Fig.8. Reinforcement as link 8 elements

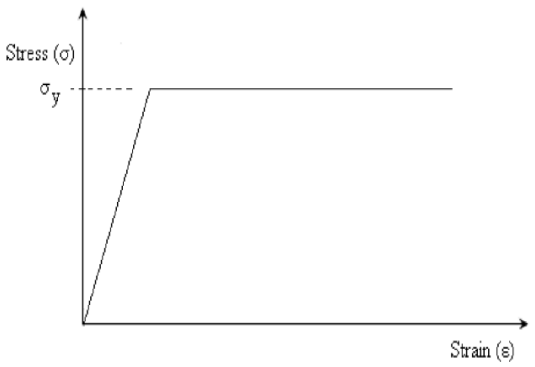

Fig.9. Plastic stress strain curve for steel meshes

Simple plastic theory was used to predict the behavior of steel sheets and the reinforcing of steel wire mesh, ignoring strain hardening. The relationship between stress and strain passes through the zero-sloping horizontal portion of the curve (see Figure 9) and continues from zero stress and strain to the yield (σ_y) point. The steel mesh and steel sheet modulus of elasticity, yield stress, and tangent modulus, also known as the strain hardening modulus, must all be defined in order to define this relationship in the program [58].

Solid 65 With and without reinforcing bars, concrete and mortar were modelled using this feature. There were eight nodes that defined this element. The degrees of freedom for every node are three. The nodal x, y, and z directions are translations of these degrees of freedom. It contains one solid material in each of the three directions, and up to three rebar materials. The rebar capability is used to represent reinforcing behavior, and the solid material is used to model concrete or mortar. The material, volume ratio, and orientation angles of reinforcement are fixed. The volume ratio is calculated by dividing the volume of rebar by the entire volume of the element. The two angles indicate the direction of the reinforcement in degrees (0 and 90) from the element coordinate system. The geometry and node positions for this element type are depicted in Figure 10 [58]. This element's ability to address nonlinear material qualities is its most significant feature. It also has great cracking and crushing capabilities. Crushing, plastic deformation, and creep are the three orthogonal directions in which the mortar and concrete might fracture. Shear is not possible for the reinforcing steel, but tensile and compression strength are. Rebar can also creep and exhibit plastic deformation.

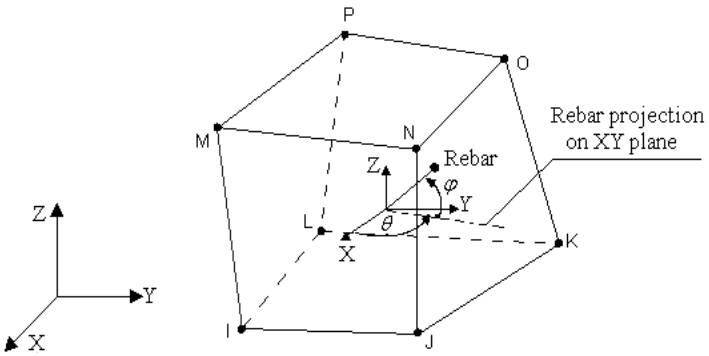

Fig.10. Geometry, node location, and the Coordinate system of solid65

Link8 is an element in the ANSYS software that simulates steel reinforcement using three different techniques: discrete, embedded, and smeared. In this investigation, the discrete model (Link8 component) was employed. A spar or truss element is the Link8 element. You may model trusses, drooping cables, links, springs, and other components with this object. The three degrees of freedom at each node of the 3D spar element are translations of nodes in the x, y, and z axes. It is a uniaxial compression element. This element does not account for the bending moment. Figure 11 [58] shows the shape, node positions, and coordinate system for this element. This component served as a model for stirrups and reinforcement bars. There isn't a true constant for this element. When the rebar is defined as a link and the rebar section area is entered, the area of the rebar cross-section can be defined. The reinforcement material that is being used is categorized as multi-linear isotropic. The Poisson ratio, or modulus of elasticity, determined how stress and strain were related in this material.

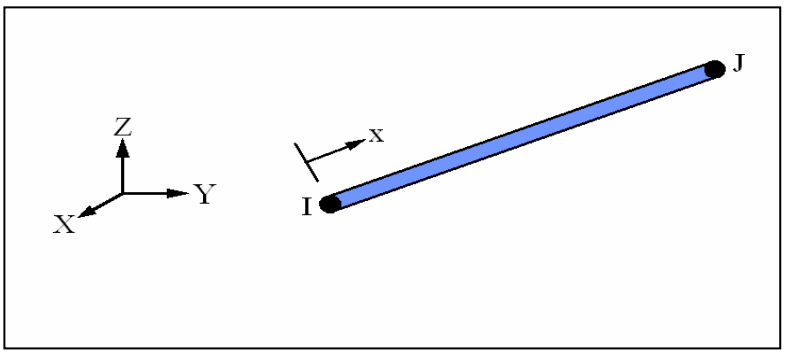

Fig 11. Link8 geometry

6. COMPARISON OF EXPERIMENTAL AND NUMERICAL RESULTS

The model of the conventional axially loaded NWC concrete column A1's collapse and failure patterns were displayed, and it was observed from the analytical results that the forms of collapse and cracking are extremely close to

the experimental data (see Figure 12). In the middle third of the column, there was an increase in crack intensity with a ratio of up to about 85% of the column's ultimate load, accompanied by numerous identical vertical cracks that formed on all of the column's faces.

The lower fulcrum area started to tilt at an angle of about 45 degrees at a load value equal to about 76% of the ultimate load value, which is when we noticed the onset of cracks in the model of a conventional NWC concrete column A2 with a bearing inner hole Axial. As weight continued, other, possibly identical fissures developed on all sides of the column. When compare the study's findings with the experimental findings, as shown in Figure 13, we find that the outcomes of the two analyses coincide quite well.

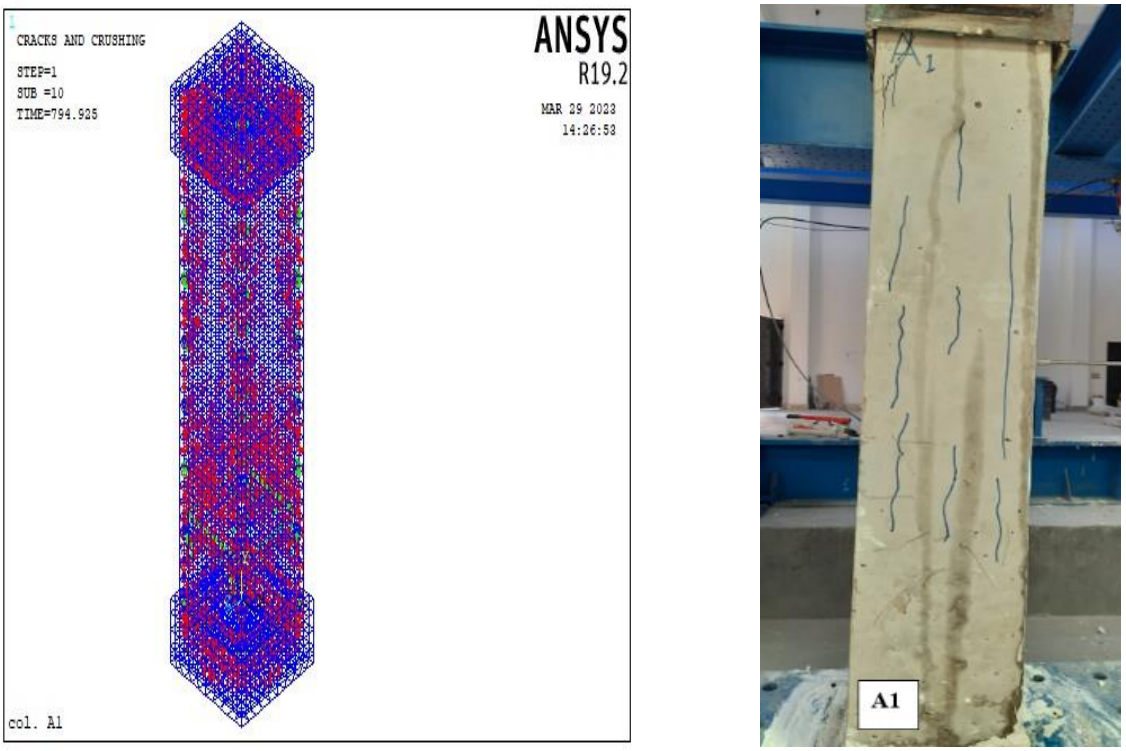

(a) Finite element. **(b) Experimental work [7].**

Fig.12. Cracks of axial loaded column (A1) as experimental and FE simulations

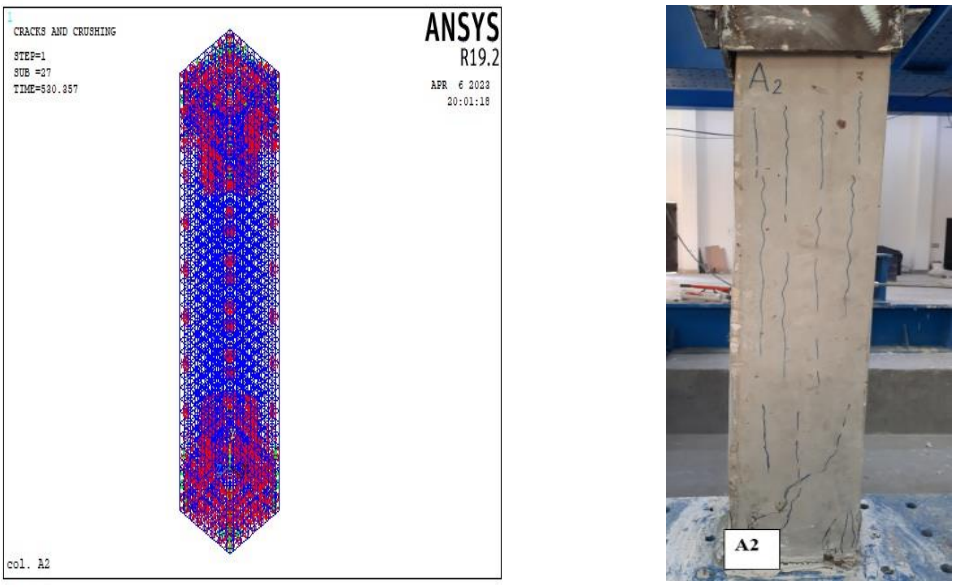

(a) Finite element. **(b) Experimental work [7].**

Fig.13. Cracks of axial loaded column (A2) as experimental and FE simulations

Figure 14 shows a comparison between the analytical results and the experimental results of the Ferrocement Concrete B1 column model with the axial bearing inner hole. I have a download value of up to 90% of the ultimate load.

We notice the beginning of the appearance of vertical cracks in the upper and lower thirds together on all sides of the column. With the continuation of increasing the loading rate, the width of the cracks began to increase significantly, accompanied by the emergence of vertical cracks in a new abundance on the ends of the column, and this is what the experimental results also concluded.

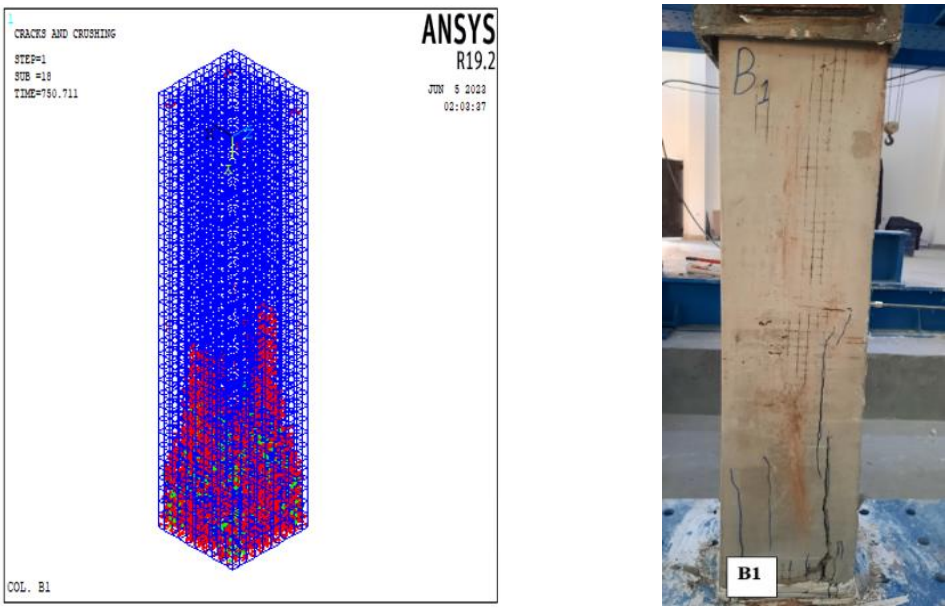

(a) Finite element. **(b) Experimental work [7].**

Fig.14. Cracks of axial loaded column (B1) as experimental and FE simulations

For models of ferrocement concrete columns with inner holes B2, B3, and B4, filled with different materials, such as BLWC, FLWC, and bricks, respectively, loaded with axial loads From the study of the analytical results, we notice that at a load value ranging from 80–90% of the ultimate load value, vertical cracks were concentrated in the upper and lower thirds together on all sides of the columns, accompanied by a concentration of stresses in the lower third of the columns. Upon reaching the load, the collapse was noticed by the multiplicity of vertical cracks on all columns. The faces of the columns indicate that these results largely coincide with the experimental results. Figures 15–17 show the breakdown patterns of the results of the two analyses together.

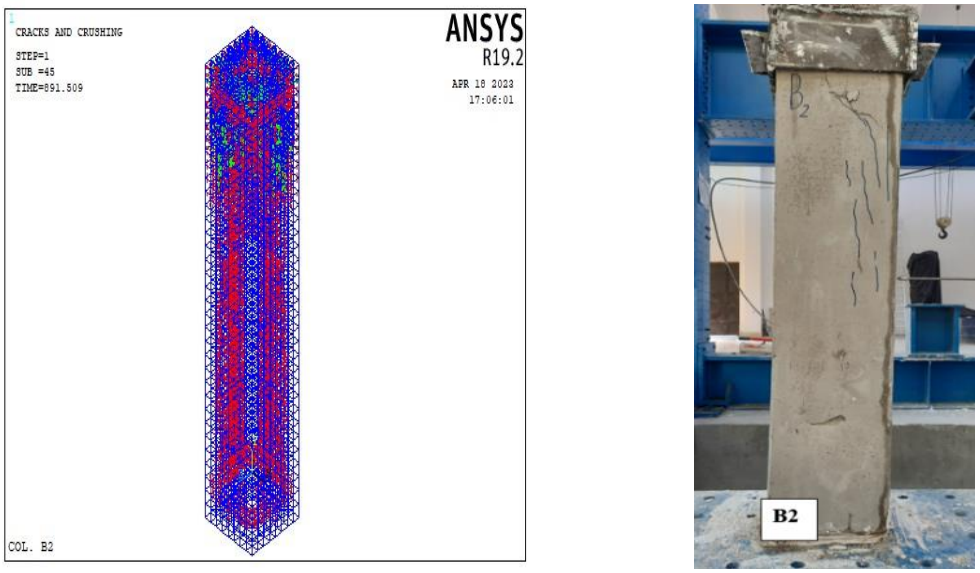

(a) Finite element. **(b) Experimental work [7].**

Fig.15. Cracks of axial loaded column (B2) as experimental and FE simulations

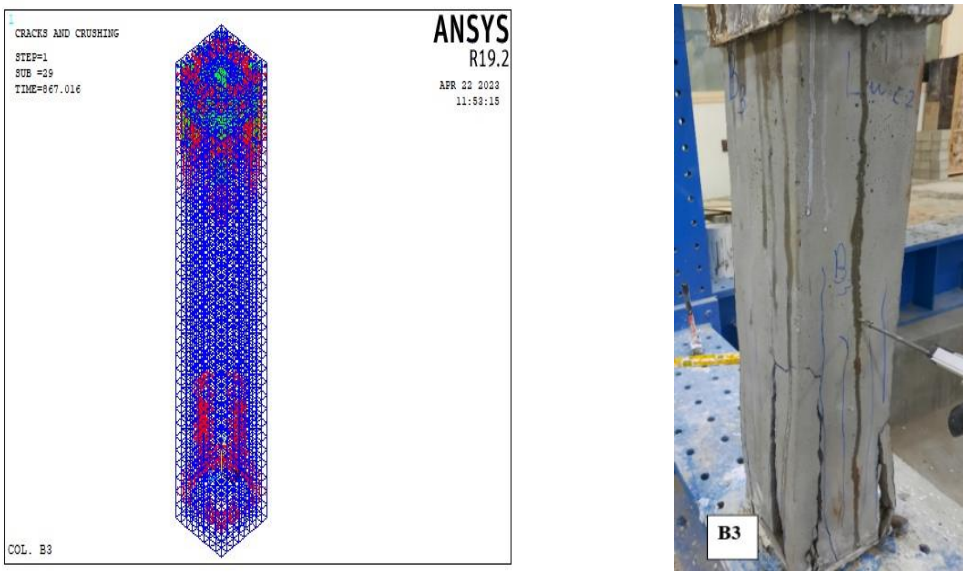

(a) Finite element. **(b) Experimental work [7].**

Fig.16. Cracks of axial loaded column (B3) as experimental and FE simulations

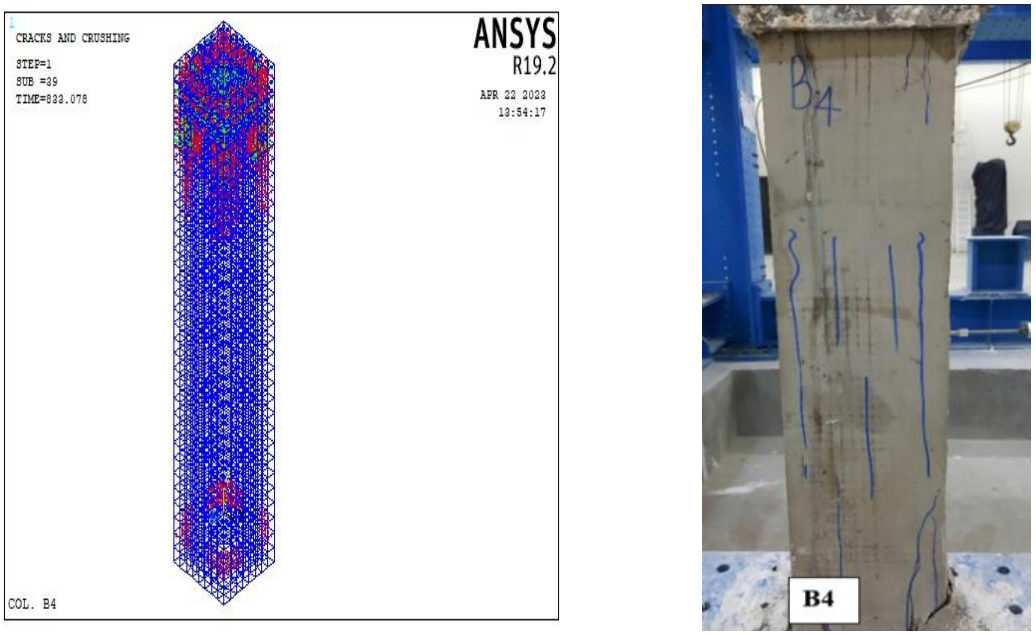

(a) Finite element. **(b) Experimental work [7].**

Fig.17. Cracks of axial loaded column (B4) as experimental and FE simulations

An analytical investigation was conducted on models of standard NWC concrete columns laden with eccentric loads, specifically column C1 solid and column C2 with a hollow inner hole, where the load was ejected from the column center by 20% of the column width. Figures 18–20 depict column C1's form and failure patterns. We see that the vertical cracks were centered in the upper third of the pressure side at a load value of around 85% of the final load value, whereas the transverse cracks were located in the middle third of the tension side. The vertical cracks extended over the entire compression side and the transverse cracks over the entire tension side upon attaining the collapse load. The backs of the slits in column C2 Vertical cracks occur on the compression side in tandem with the transverse load on the tension side, but at a load value that is almost 75% of the ultimate load value. The hole inside the column is the cause of the load rate drop. A comparison of the analytical data of columns C2 is displayed in Figures 21–23. when compare the experimental results and analytical results, find that they are somewhat identical.

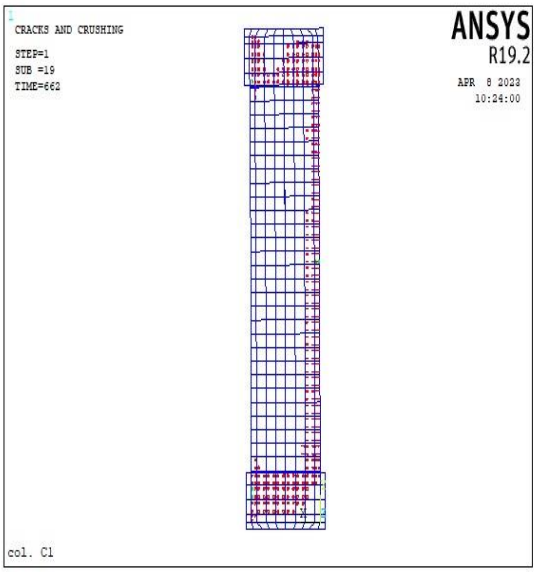

(a) Finite element. **(b) Experimental work [7].**

Fig.18. Cracks of eccentric loaded column at tension face (C1) as experimental and FE simulation.

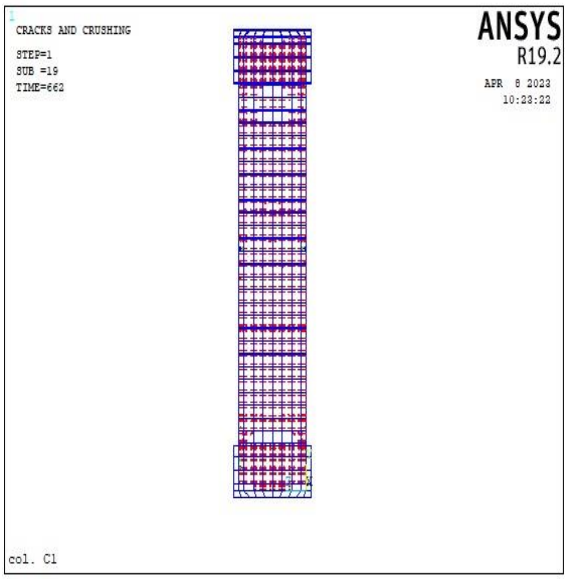

(a) Finite element. **(b) Experimental work [7].**

Fig.19. Cracks of the eccentric loaded column at compression face (C1) as experimental and FE simulations

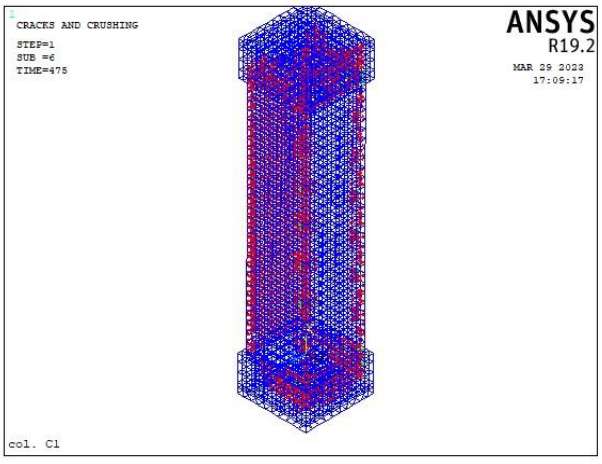

Fig.20. Cracks of eccentric loaded column (C1) as FE simulations

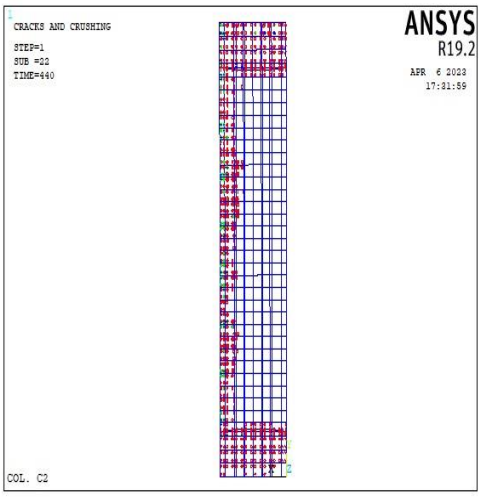

(a) Finite element. **(b) Experimental work [7].**

Fig.21. Cracks of eccentric loaded column at tension face (C2) as experimental and FE simulations

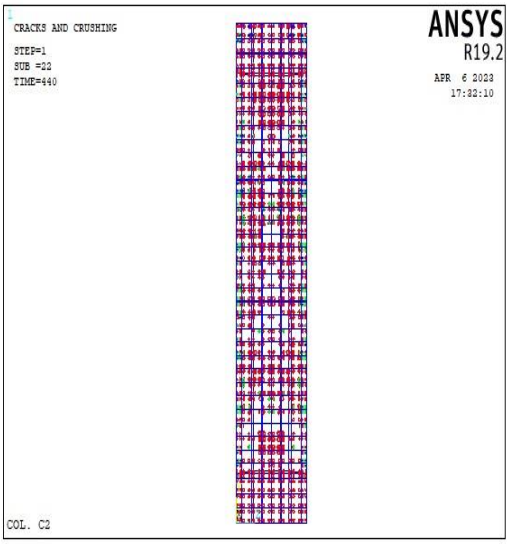

(a) Finite element. **(b) Experimental work [7].**

Fig.22. Cracks of eccentric loaded column at compression face (C2) as experimental and FE simulations

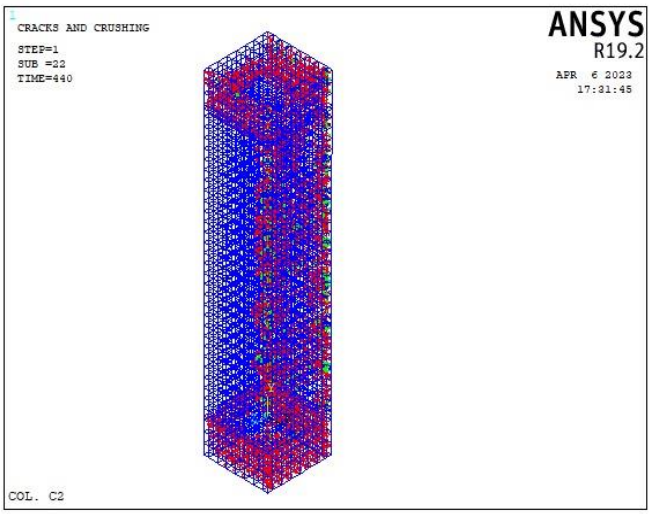

Fig.23. Cracks of eccentric loaded column (C2) as FE simulations

An eccentric load was applied to the ferrocement concrete columns with inner holes D1, D2, and D3 filled with lightweight mixes, such as BLWC and FLWC and bricks, respectively. The analytical results demonstrated that, at a load value of roughly 90% of the ultimate load, the transverse cracks were concentrated in the middle third of the column on the opposite side of the load relay, while the vertical cracks were concentrated in the upper and lower thirds of the column together in the direction of the load relay. Samples D1, D2, and D3 exhibit cracks, as seen in Figures 24–32. The analytical and experimental results noticed agreement in the failure patterns and crack shapes of the analytical and experimental results of the columns.

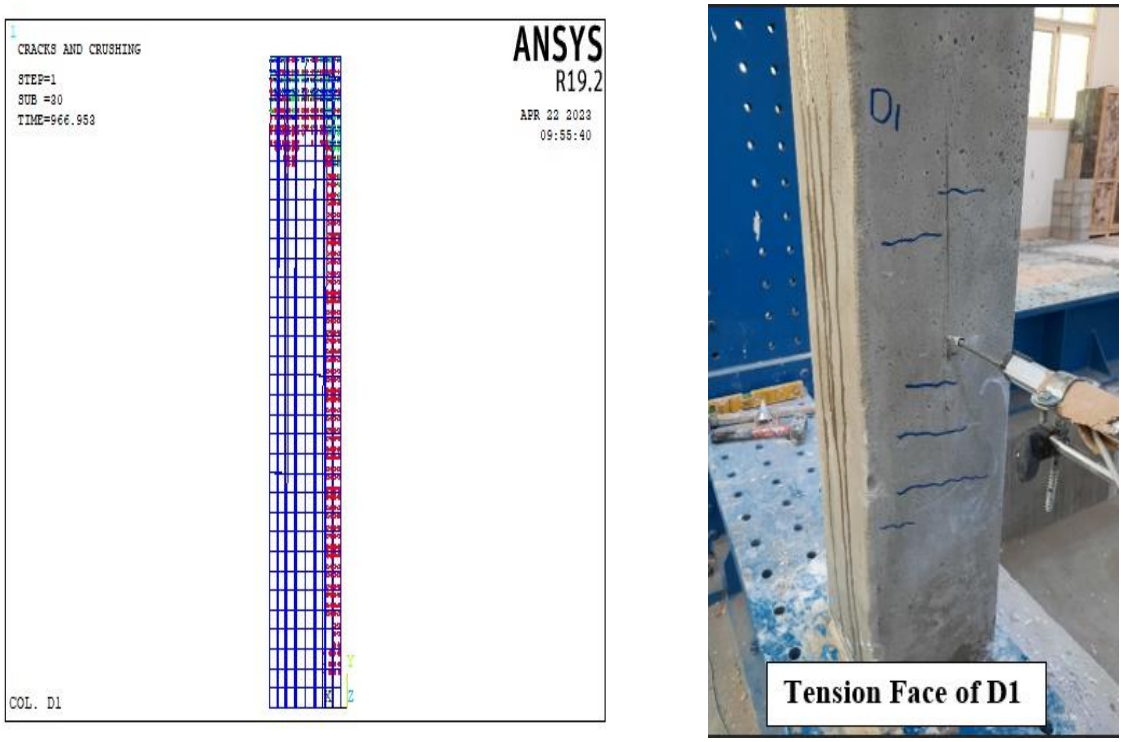

(a) Finite element. **(b) Experimental work [7].**

Fig.24. Cracks of eccentric loaded column at tension face (D1) as experimental and FE simulations

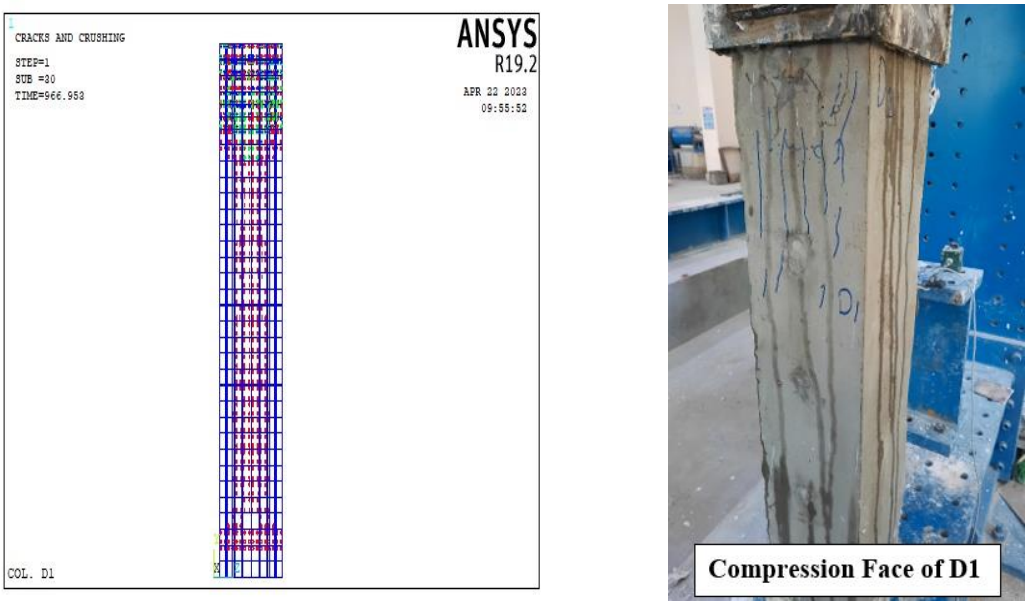

(a) Finite element. **(b) Experimental work [7].**

Fig.25. Cracks of eccentric loaded column at compression face (D1) as experimental and FE simulations

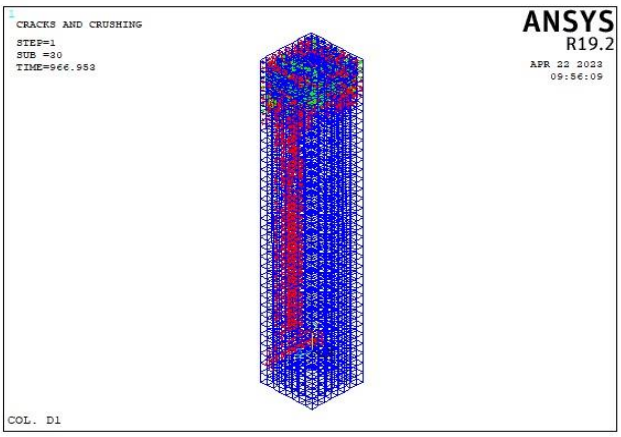

Fig.26. Cracks of eccentric loaded column (D1) as FE simulations

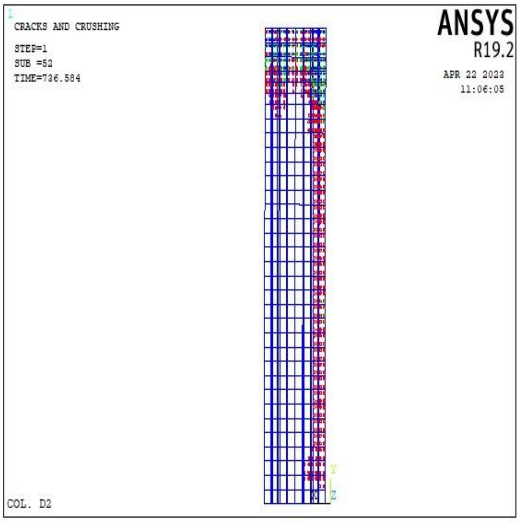

(a) Finite element.

(b) Experimental work [7].

Fig.27. Cracks of eccentric loaded column at tension face (D2) as experimental and FE simulations

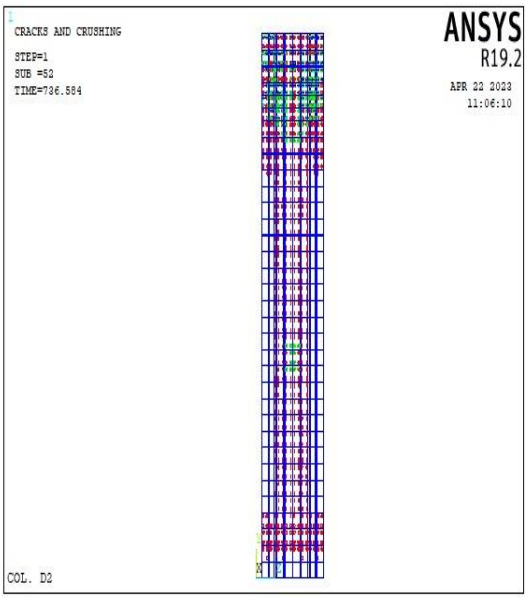

(a) Finite element.

(b) Experimental work [7].

Fig.28. Cracks of eccentric loaded column at compression face (D2) as experimental and FE simulations

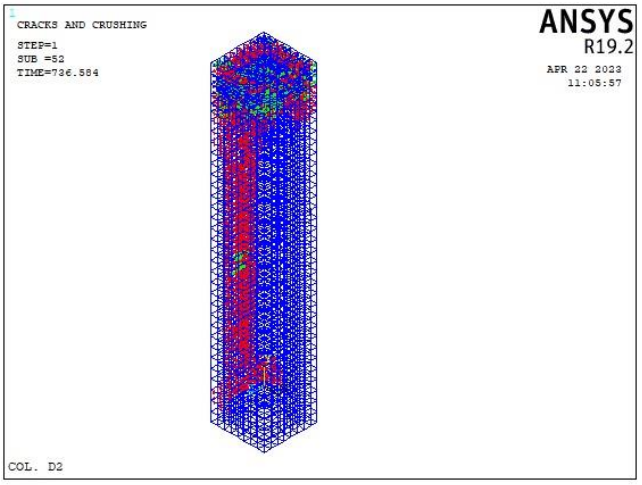

Fig.29. Cracks of eccentric loaded column (D2) as FE simulations

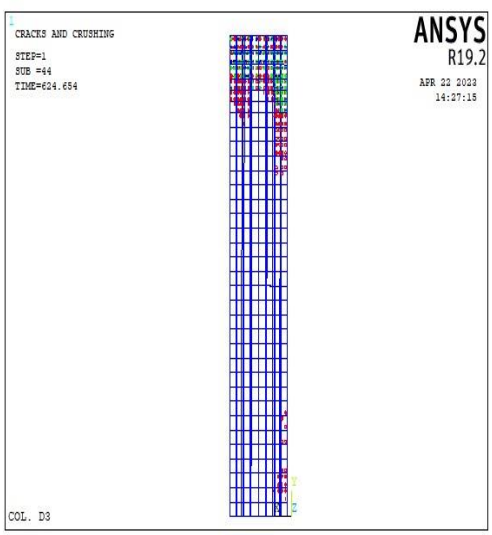

(a) Finite element.

(b) Experimental work [7].

Fig.30. Cracks of eccentric loaded column at tension face (D3) as experimental and FE simulations

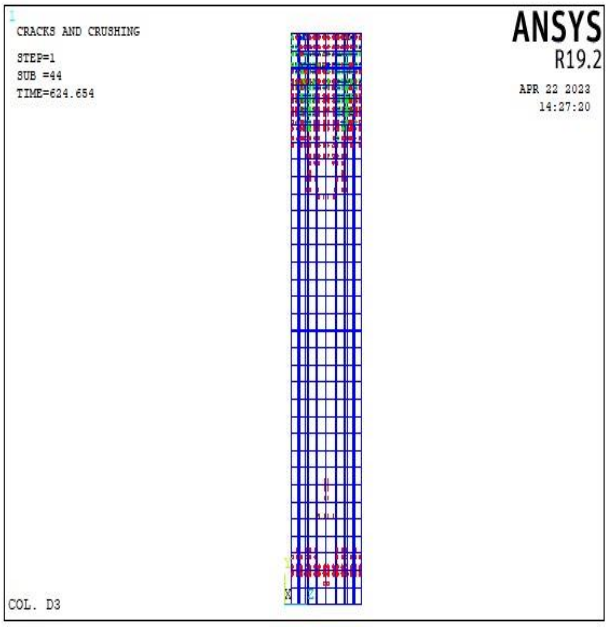

(a) Finite element.

(b) Experimental work [7].

Fig.31. Cracks of eccentric loaded column at compression face (D3) as experimental and FE simulations

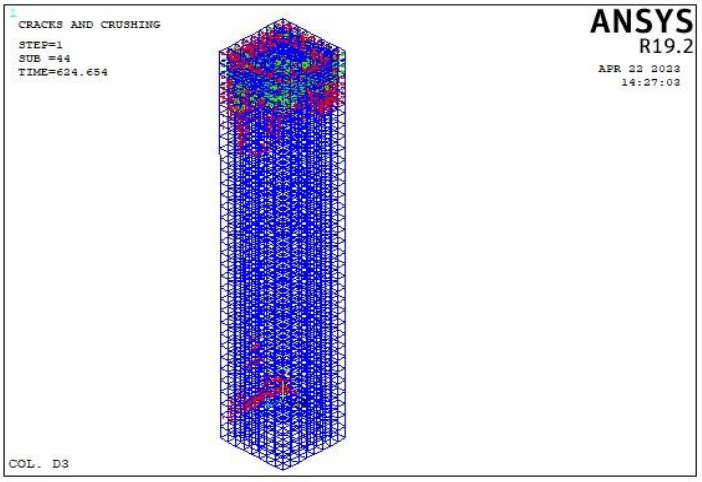

Fig.32. Cracks of eccentric loaded column (D3) as FE simulations

It was determined how the load and vertical displacement curves of typical NWC concrete columns related to each other as well as to the load and horizontal displacement curves. under the effect of an axial load, as seen in samples A1 and A2, respectively, having a solid core and an inner hole. When the load reaches 50% of the maximum load value, the results of the analytical work are applied to the experimental curve for sample A1 of the load and vertical displacement curves. However, once the load reaches the breaking point, the vertical and horizontal displacement for the analytical work decreased by 8.37 and 12.9%, respectively, in comparison to the experimental results displayed in Figure 33. Regarding sample A2, we note that the load and vertical displacement curves are similar in relation to the results of the two analyses, as the difference between the final displacement values between them was 3.06%. On the other hand, the horizontal displacement decreased by 21.27%. This is due to the nonlinearity of the analytical results curve, as shown in Figure 34.

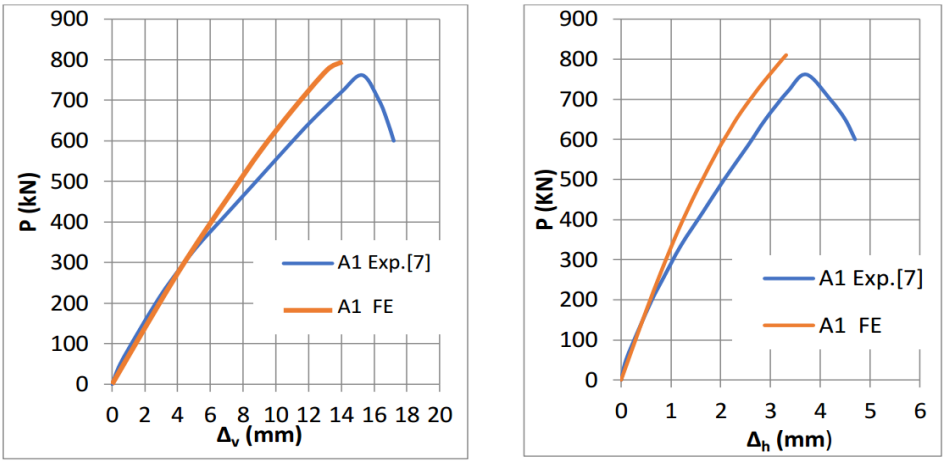

Fig.33. Load-displacement curves of axial loaded column (A1)

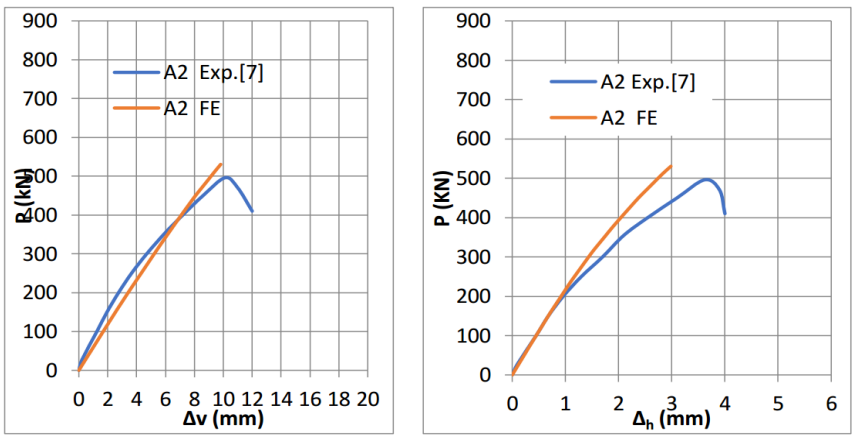

Fig.34. Load-displacement curves of axial loaded column (A2)

For the axially loaded FC columns—represented by the inner-hole specimens B1, B2, B3, and B4 filled with lightweight BLWC, FLWC, and bricks, respectively—the values of the changes in the relationship between the load curves and the vertical displacement and the load curves and the horizontal displacement at the end of the load were observed. In sample B1, the analytical work's vertical and horizontal displacement values were 19.34 and 12.36% lower than the experimental work's findings, respectively. In contrast, the analytical work's ultimate load value was 4% higher than the experimental results (refer to Figure 35). In comparison to the experimental results, the vertical displacement values for samples B2, B3, and B4 increased by 30.23, 27.85, and 4.38%, respectively, according to the analytical results. On the other hand, the horizontal displacement values increased by 64, 56.27, and 16.95%, respectively, corresponding to a slight increase in ultimate load for the samples at a rate of 0.97, 0.11, and 3.08%, respectively, compared to the results of the experimental work as shown in Figures 36–38.

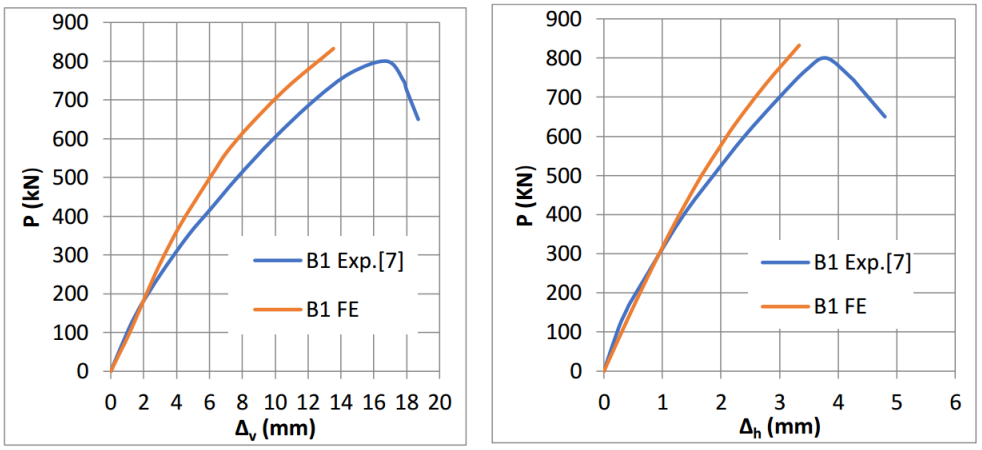

Fig.35. Load-displacement curves of axial loaded column (B1)

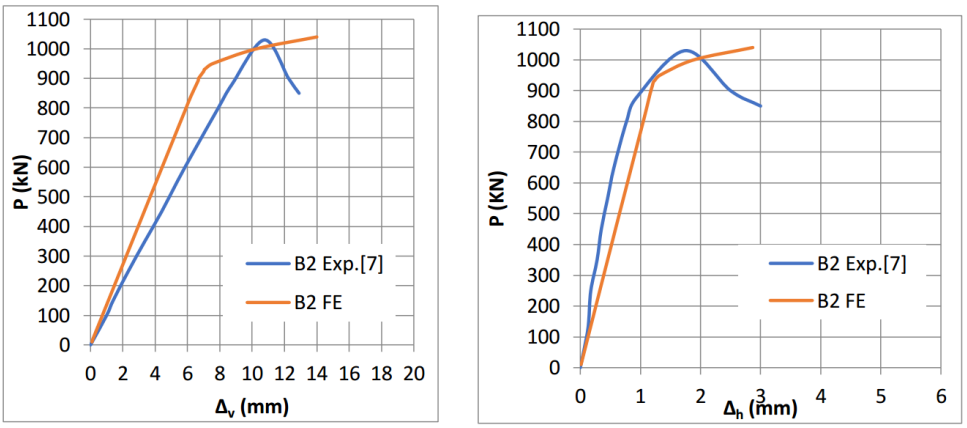

Fig.36. Load-displacement curves of axial loaded column (B2)

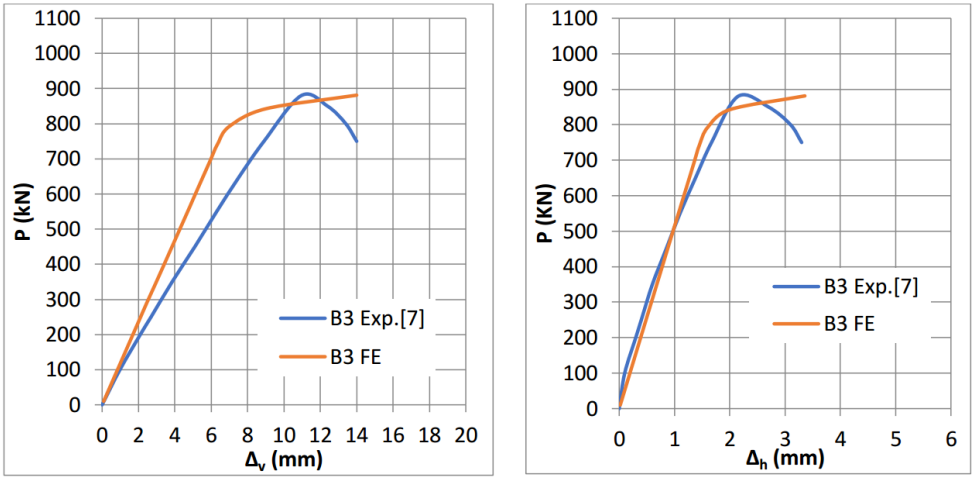

Fig.37. Load-displacement curves of axial loaded column (B3)

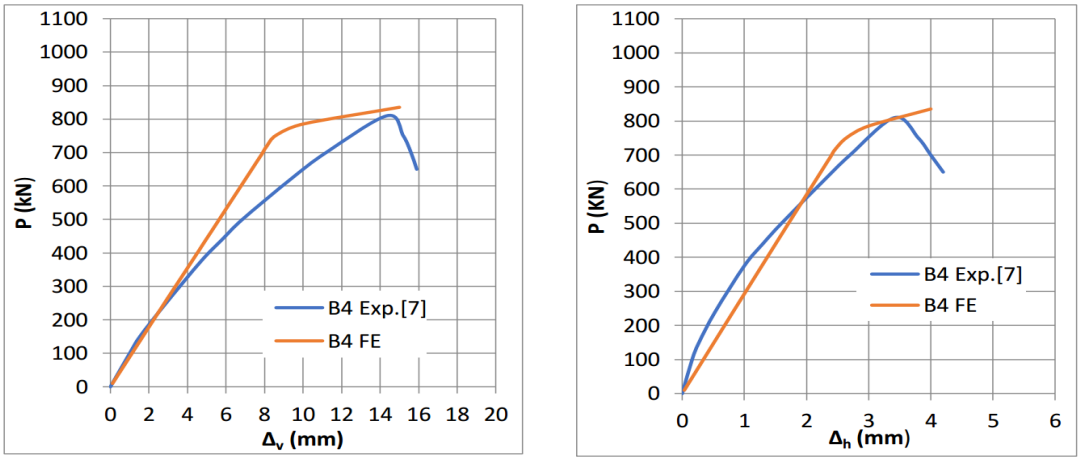

Fig.38. Load-displacement curves of axial loaded column (B4)

For NWC columns, represented in sample C1 with a solid core and sample C2 with an internal hole, under the influence of the eccentric load, we note from the curves of load and vertical displacement, in addition to the curves of load and horizontal displacement of columns C1 and C2 that the results of the analytical work apply to some extent with the results of the experimental work (see Figures 39, 40), as the vertical displacement values for the analytical work decreased by 9.6 and 5.1%, while the horizontal displacement values for the analytical work decreased by 3.83 and 7.59%, respectively, when the ultimate load for the analytical work of the columns increased by 1.35 and 0.68% for both samples compared to the experimental results.

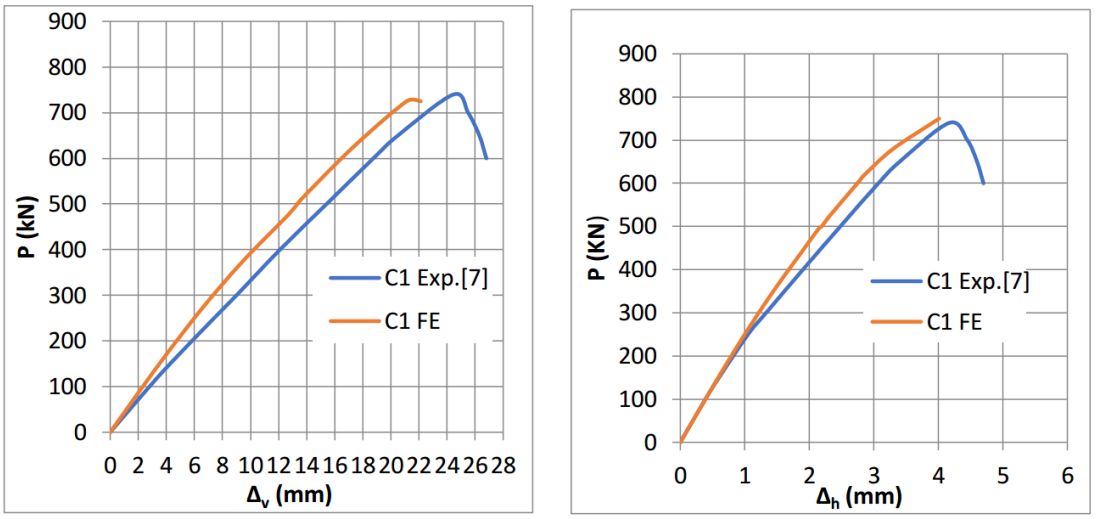

Fig.39. Load-displacement curves of eccentric loaded column (C1)

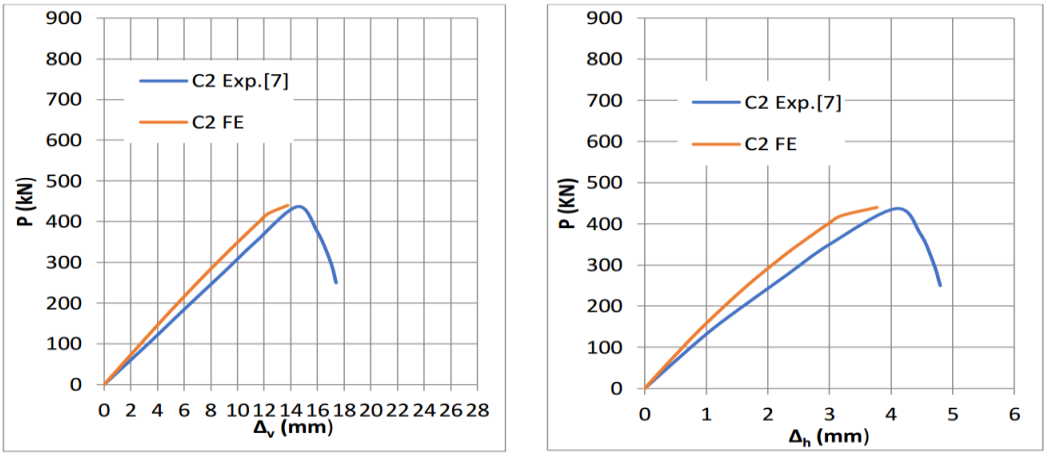

Fig.40. Load-displacement curves of eccentric loaded column (C2)

Samples D1, D2, and D3, which represent FC columns, were evaluated with an eccentric load (20% of the column width) applied to them. The interior hole of these columns was filled with lightweight BLWC, FLWC, and bricks. A comparison of the outcomes of the two analyses combined for these columns can be seen in Figures 41–43. The displacement values for the analytical work increased by 5.51 and 15%, respectively, from the load curves and the vertical displacement of columns D1 and D2 but reduced by 3.53% for column D3. Conversely, when the ultimate load for the analytical work of the columns increased by 3.75, 0.79, and 2.29% for both samples in comparison to the experimental results, the horizontal displacement values for the columns increased by 0, 25.78, and 13.08%, respectively.

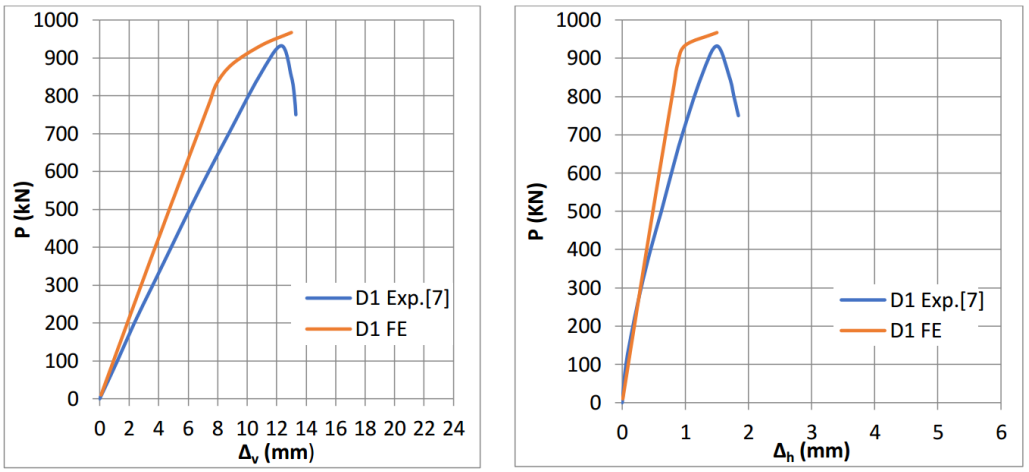

Fig.41. Load-displacement curves of eccentric loaded column (D1)

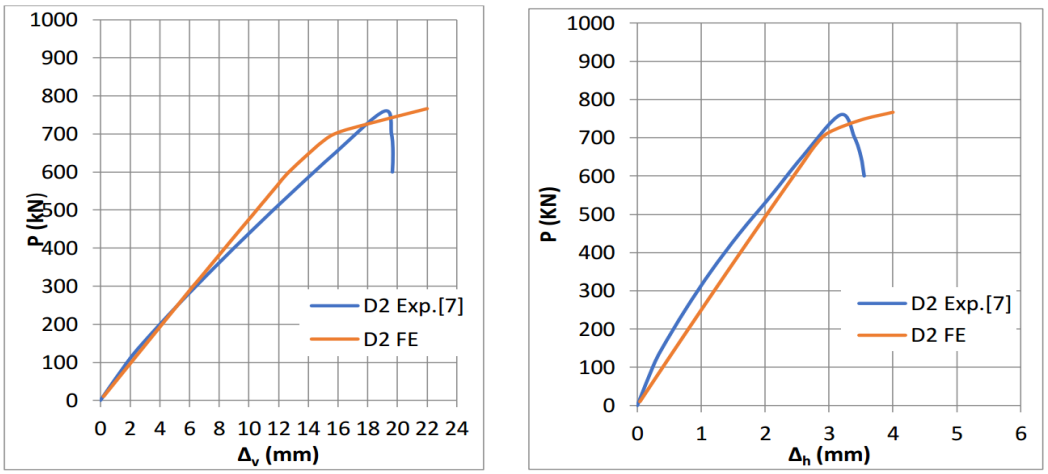

Fig.42. Load-displacement curves of eccentric loaded column (D2)

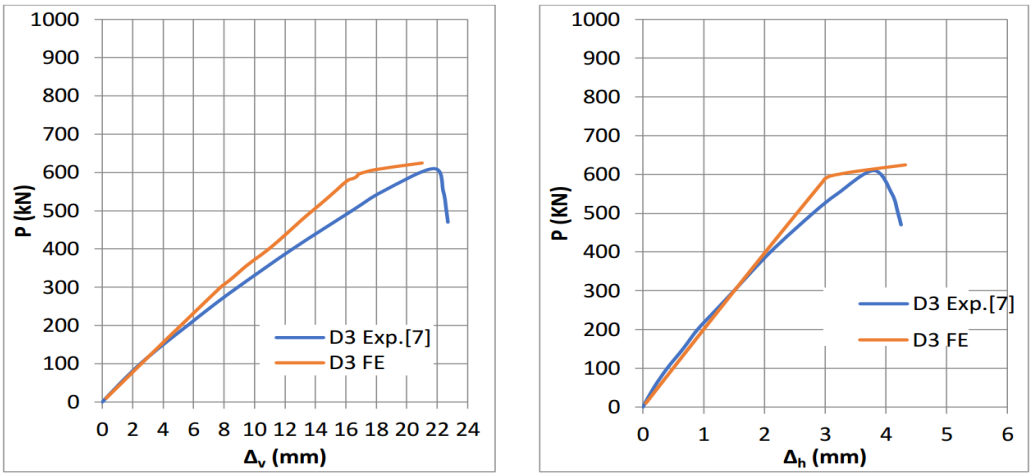

Fig.43. Load-displacement curves of eccentric loaded column (D3)

The ultimate load (Pu) of the column samples and the values of vertical displacement (ΔV) and horizontal displacement (Δh) corresponding to the ultimate load result of the experimental and analytical work are provided in Table 6, which compares the experimental and analytical results. When compared to the findings of the experimental work, observed a small rise in the loads' value as a result of the analytical work; the percentage of increase varies from 0.11% to 4.19%. Regarding the variation in the vertical displacement value, observed that, in comparison to the experimental work's results, certain columns cause the value of the analytical work's results to drop by a rate ranging from 3.68% to 19.34%, and other columns cause an increase by a rate ranging from 4.38% to 30.23%. Regarding the variation in the horizontal displacement value, we observe that, in comparison to the experimental work's results, certain columns cause a value of the analytical work's results to drop by a rate ranging from 0% to 21.27%, while other columns cause the value to increase by a rate ranging from 0% to 56.27%. also noticed, by comparing the experimental and theoretical results, that the percentage of difference between them is rather low.

Table 6: Results analysis at ultimate load, vertical displacement, and horizontal displacement for samples

Sample	Ultimate Load (Pu)			Vertical displacement at ultimate load (ΔV)			horizontal displacement at ultimate load (Δh)		
	Experimental results (kN)	Finite element results (kN)	Change in Pu (%)	Experimental results (mm)	Finite element results (mm)	Change in Δv (%)	Experimental results (mm)	Finite element results (mm)	Change in Δh (%)
A1	762	794	4.19	15.28	14	-8.37	3.72	3.24	-12.9
A2	496	510	2.82	10.12	9.81	-3.06	3.62	2.85	-21.27
B1	800	832	4	16.8	13.55	-19.34	3.8	3.33	-12.36
B2	1030	1040	0.97	10.75	14	30.23	1.75	2.87	64
B3	880	881	0.11	10.95	14	27.85	2.15	3.36	56.27
B4	810	835	3.08	14.37	15	4.38	3.42	4	16.95
C1	740	750	1.35	24.47	22.12	-9.6	4.17	4.01	-3.83
C2	437	440	0.68	14.5	13.76	-5.1	4.08	3.77	-7.59
D1	932	967	3.75	12.32	13	5.51	1.5	1.5	0
D2	760	766	0.79	19.12	22	15	3.18	4	25.78
D3	610	624	2.29	21.77	21	-3.53	3.82	4.32	13.08

Note: Change in Pu (%), change in Δv (%) and change in Δh equal ((Finite element results - Experimental results)/ Experimental results) ×100

7. CONCLUSIONS

Experimental research has previously examined the structural performance of lightweight hollow box columns filled with various lightweight materials. The main influencing factors are the type of lightweight concrete used for the hollow core, the concrete itself, the current steel mesh fabric welded wire mesh, and the loading system, which includes both axial and eccentric loads. In this study, the ultimate load and maximum vertical and horizontal displacements of the tested ferrocement and conventional concrete columns were predicted using finite element models and ANSYS V19 software. The samples were loaded until failure happened, and the experimental and finite element model findings for the tested columns were compared. The efficiency of the used model was confirmed by comparing the final loads, the fracture pattern, and the displacements' reaction to the load by comparing the finite element models with the experimental data.

The behaviour of the tested columns is displayed in the testing results of the experimental programme and the finite element method in the current study. Following the findings, the following conclusions were made:

(1) Compared to conventional concrete samples of normal weight, the ferrocement samples that were examined under axial and eccentric compressive stresses demonstrated larger ultimate loads.

(2) The results of the tests indicated that using WWM filler materials for FC ferrocement columns lowers the displacement values of the hole control column and enhances the behaviour of the specimens to withstand ultimate loads.

(3) Ferrocement columns FC containing BLWC have a larger ultimate load Pu than columns containing FLWC and bricks under axial and eccentric compressive loads because BLWC is stronger than FLWC and bricks.

(4) The results demonstrated that, in comparison to the ferrocement control columns loaded with axial load, the load deflection by 20% displacement of the sample width reduces the ultimate load of FC columns by an average of 16% and increases the values of horizontal and vertical displacements by an average of 46.7 and 24.43%, respectively.

(5) The ratio between the vertical displacements of the experimental and analytical findings ranged from 5.1% to 19.34%, and the ratio between the experimental and analytical ultimate loads ranged from 0.68 to 4.19% when comparing the results produced by FE and experimental models. The horizontality of the experimental and analytical results ranged from 3.83% to 21.27% in the displacement ratio. The finite element model's ability to forecast the test samples' ultimate load is validated by these findings. It is evident that there is good agreement between the experimental values and the theoretical model's value and the finite element.

REFERENCES

[1] ACI Committee 549, State of the Art Report on Ferrocement, ACI 549–R97, in Manual of Concrete Practice, ACI, Detroit, 1997, pp.26.

[2] ACI Committee 549-IR-93, Guide for the Design, Construction and Repair of Ferrocement, ACI 549-IR-88 and IR 93, in Manual of Concrete Practice, American Concrete Institute, Farmington Hills, Michigan, 1988 and 1993, p. 27.

[3] Naaman AE. Ferrocement and laminated cementitious composites. Ann Arbor, Michigan: Techno Press 3000; 2000. p. 372.

[4] Aboul-Anen B, El-Shafey A, El-Shami M (2009). Experimental and analytical model of ferrocement slabs. International Journal of Recent Trends in Engineering, 1(6), 25-29.

[5] Al-Kubaisy MA, Jumaat MZ (2000). Flexural behavior of reinforced concrete slabs with ferrocement tension zone cover. Construction and Building Materials, 14(5), 245-252.

[6] Elavenil S, Chandrasekar V (2007). Analysis of reinforced concrete beams strengthened with ferrocement. International Journal of Applied Engineering Research, 2(3), 431- 440.

[7] Eltaly, B. A., Shaheen, Y. B., EL-boridy, A. T., & Fayed, S. (2023). Ferrocement composite columns incorporating hollow core filled with lightweight concrete. Engineering Structures, 280, 115672.

[8] Shaheen, Y. B., Eltaly, B. A., Yousef, S. G., & Fayed, S. (2023). Structural performance of ferrocement beams incorporating longitudinal hole filled with lightweight concrete. International Journal of Concrete Structures and Materials, 17(1), 21.

[9] Shaheen, Yousry BI, B. Eltaly, and S. Abdul-Fataha. "Structural performance of ferrocement beams reinforced with composite materials." Structural Engineering and Mechanics 50.6 (2014): 817-834.

[10] Fahmy, E. H., Shaheen, Y. B., Abdelnaby, A. M., & Abou Zeid, M. N. (2014). Applying the ferrocement concept in construction of concrete beams incorporating reinforced mortar permanent forms. International Journal of Concrete Structures and Materials, 8, 83-97.

[11] Shaaban, I. G., Shaheen, Y. B., Elsayed, E. L., Kamal, O. A., & Adesina, P. A. (2018). Flexural characteristics of lightweight ferrocement beams with various types of core materials and mesh reinforcement. Construction and Building materials, 171, 802-816.

[12] Shaaban, I. G., Shaheen, Y. B., Elsayed, E. L., Kamal, O. A., & Adesina, P. A. (2018). Flexural behaviour and theoretical prediction of lightweight ferrocement composite beams. Case studies in construction materials, 9, e00204.

[13] Sakthivel, P.B.; Jagannathan, A. Fiber reinforced ferrocement—A review study. In Proceedings of the 2nd International Conference on Advances in Mechanical, Manufacturing and Building Sciences (ICAMB-2012), Vellore, India, 9–11 January 2012; pp. 1172–1177

[14] Navid, S.S.; Bhalsing, S.S.; Pankaj, B.A. Tensile strength of ferrocement with respect to specific surface. Int. J. Eng. Adv. Technol. 2013, 3, 473–475.

[15] Kumar, A. Ferrocement box sections-viable option for floors and roof of multi-story buildings. Asian J. Civil Eng. Build. Hous. 2005, 6, 569–582.

[16] Rajendran, M.; Soundarapandian, N. Geopolymer ferrocement panels under flexural loading. Sci. Eng. Compos. Mater. 2015, 22, 331–341.

[17] Vicridge, I.G.; Ranjabar, M.M. The effect of aggressive environment on the flexural performance of ferreocement. In Proceedings of the 6th International Symposium on Ferrocement, Ann Arbor, MI, USA, 7–10 June 1998; pp. 313–328.

[18] Vickridge, I.G.; Ranjbar, M.M. The combined effect of crack, load and aggressive environment on the corrosion rate of ferrocement reinforcement. In Proceedings of the 6th International Symposium on Ferrocement, Ann Arbor, MI,

USA, 7–10 June 1998; pp. 329–343.
[19] Dotto, J.M.R.; De Abreu, A.G.; Dal Molin, D.C.C.; Müller, I.L. Influence of silica fume addition on concrete physical properties and on corrosion behaviour of reinforcing bars. Cem. Concr. Compos. 2004, 26, 31–39.
[20] Torri, K.; Kawamura, M. Chloride induced corrosion of steel reinforcement made with various mineral admixtures. Trans. Jpn. Conc. Inst. 1990, 12, 183–190.
[21] S. D. S. R. Thenmozhi and S. D. Shri, "An Experimental investigation on the flexural behavior of scc ferrocement slabs incorporating fibers," International Journal of Engineering Science and Technology (IJEST), 2012.
[22] A. W. Hago, K. S. Al-Jabri, A. S. Alnuaimi, H. Al-Moqbali, and M. A. Al-Kubaisy, "Ultimate and service behavior of ferrocement roof slab panels," Construction and Building Materials, vol. 19, no. 1, pp. 31–37, 2005.
[23] Fayed, S. (2019). Flexural Strengthening of Defected RC Slabs Using Strain-Hardening Cementitious Composites (SHCC): An Experimental Work. Arabian Journal for Science and Engineering, 1-12.
[24] Basha, A., Fayed, S., & Mansour, W. (2020). Flexural strengthening of RC one way solid slab with Strain Hardening Cementitious Composites (SHCC). Advances in concrete construction, 9(5), 511-527.
[25] Mansour, W. & Fayed, S. (2021). Effect of interfacial surface preparation technique on bond characteristics of both NSC-UHPFRC and NSC-NSC composites. Structures, 29, 147–166.
[26] Baraghith, A. T., Mansour, W., Behiry, R. N., & Fayed, S. (2022). Effectiveness of SHCC strips reinforced with glass fiber textile mesh layers for shear strengthening of RC beams: Experimental and numerical assessments. Construction and Building Materials, 327, 127036.
[27] Fayed, S., Badr el-din, A., Basha, A., & Mansour, W. (2022). Shear behavior of RC pile cap beams strengthened using ultra-high performance concrete reinforced with steel mesh fabric. Case Studies in Construction Materials, 17, e01532.
[28] Mansur, M. A., and P. Paramasivam. "Ferrocement short columns under axial and eccentric compression." Structural Journal 87.5 (1990): 523-529.
[29] Sirimontree, Sayan, Boonsap Witchayangkoon, and Krittiya Lertpocasombut. "Strengthening of reinforced concrete column via ferrocement jacketing." American Transactions on Engineering and Applied Sciences 4.1 (2015): 39-47.
[30] El-Kholy, Ahmed M., and Hany A. Dahish. "Improved confinement of reinforced concrete columns." Ain Shams Engineering Journal 7.2 (2016): 717-728.
[31] Shaheen1a, Yousry BI, Ashraf M. Mahmoud, and Hala M. Refat3b. "Experimental and FE simulations of ferrocement columns incorporating composite materials." Structural Engineering and Mechanics 64.2 (2017): 155-171.
[32] Shaheen, Y. B., Etman, Z. A., & Ramadan, A. G. (2016). Structural Behavior of Light Weight Ferrocement Columns. Concrete Research Letters, 7(1).
[33] Mahmoud, Akram S., Sinan A. Yaseen, and Samar S. Shafeeq. "Strengthening and Retrofitting of Reinforced Concrete Hollow Columns using High Strength Ferrocement Fibers Composites." Al-Nahrain Journal for Engineering Sciences 20.3 (2017): 625-635.
[34] Kondraivendhan, B., and Bulu Pradhan. "Effect of ferrocement confinement on behavior of concrete." Construction and Building Materials 23.3 (2009): 1218-1222.
[35] Ravichandran, K., and C. Antony Jeyasehar. "Seismic retrofitting of exterior beam column joint using ferrocement." International Journal of Engineering and Applied Sciences 4.2 (2012): 35-58.
[36] Ganesan, N., P. V. Indira, and S. P. Thadathil. "Effect of ferrocement wrapping system on strength and behavior of RC frames under reversed lateral cyclic loading." Experimental Techniques 35.4 (2011): 23-28.
[37] Singh, K. K., and S. K. Kaushik. "Behaviour of ferrocement composite columns in compression." ACI international conference on high performance concrete, design and materials and recent advances in concrete technology, Kuala Lumpur. 1997.
[38] Kaish, A. A., Alam, M. R., Jamil, M., & Wahed, M. A. (2013). Ferrocement jacketing for restrengthening of square reinforced concrete column under concentric compressive load. Procedia Engineering, 54, 720-728.
[39] Li, X., Xie, H., Yan, M., Gou, H., Zhao, G., & Bao, Y. (2018). Eccentric compressive behavior of reinforced concrete columns strengthened using steel mesh reinforced resin concrete. Applied Sciences, 8(10), 1827.
[40] Soman, Mini, and Jebin Mohan. "Rehabilitation of RC columns using ferrocement jacketing." Construction and Building materials 181 (2018): 156-162.
[41] Xiong, G. J., Wu, X. Y., Li, F. F., & Yan, Z. (2011). Load carrying capacity and ductility of circular concrete columns confined by ferrocement including steel bars. Construction and Building Materials, 25(5), 2263-2268.
[42] Mabrouk, Rasha, et al. "Strengthening of reinforced concrete short columns using ferrocement under axial loading." Journal of Engineering Research 6.3 (2022): 32-48.
[43] Abdullah, and Katsuki Takiguchi. "An investigation into the behavior and strength of reinforced concrete columns strengthened with ferrocement jackets." Cement and Concrete Composites 25.2 (2003): 233-242.
[44] Mourad, S. M., and M. J. Shannag. "Repair and strengthening of reinforced concrete square columns using ferrocement jackets." Cement and concrete composites 34.2 (2012): 288-294.

[45] Kaish, A. A., Alam, M. R., Jamil, M., & Wahed, M. A. (2013). Ferrocement jacketing for restrengthening of square reinforced concrete column under concentric compressive load. Procedia Engineering, 54, 720-728.
[46] Aboul-Anen, B., El-Shafey, A., & El-Shami, M. (2009). Experimental and analytical model of ferrocement slabs. International Journal of Recent Trends in Engineering, 1(6), 25.
[47] Shaheen, Y. B. I., Eltaly, B., & Kameel, M. (2013). Experimental and analytical investigation of ferrocement water pipe. Journal of Civil Engineering and Construction Technology, 4(4), 157-167.
[48] Shaheen, Y. B., Eltaly, B. A., & Hanesh, A. A. (2014). Experimental and FE simulations of Ferrocement Domes Reinforced with Composite Materials. Concrete Research Letters, 5(4).
[49] El-Taly, B. (2018). Retrofitting notch damaged box steel beams with composite materials. KSCE Journal of Civil Engineering, 22(8), 3003-3014.
[50] El-Taly, B. (2016). Structural performance of notch damaged steel beams repaired with composite materials. International Journal of Advanced Structural Engineering (IJASE), 8(2), 119-131.
[51] Nawar, M., Elshafy, A., Eltaly, B., & Kandil, K. (2021). Experimental and Numerical Analysis of Steel Beam-Column Connections. ERJ. Engineering Research Journal, 44(1), 43-49.
[52] Eltaly, B., Saudi, G., Ali, R., & Kandil, K. (2014). Experimental and FE modal analysis for elevated steel water tanks. International Journal of Engineering Research & Technology (IJERT) Volume, 3.
[53] Al-Nuaimi, A. S., & Bhatt, P. (2005). 2D idealisation of hollow reinforced concrete beams subjected to combined torsion, bending and shear. The Journal of Engineering Research [TJER], 2(1), 53-68.
[54] Hauhnar, L., Rajkumar, R., & Umamaheswari, N. (2017). Behavior of reinforced concrete beams with circular opening in the flexural zone strengthened by steel pipes. Int. J. Civ. Eng. Technol, 5, 303-309.
[55] Hassan, N. Z., Ismael, H. M., & Salman, A. M. (2018). Study behavior of hollow reinforced concrete beams. Int. J. Curr. Eng. Technol, 8(6), 1640-1651.
[56] Elamary, A. S., Sharaky, I. A., & Alqurashi, M. (2021, August). Flexural behaviour of hollow concrete beams under three points loading: Experimental and numerical study. In Structures (Vol. 32, pp. 1543-1552). Elsevier.
[57] AISC (American Institute of Steel Construction). (2010). "Specification for structural steel buildings." AISC 360-10, Chicago.
[58] Ibrahim, A. M., Mohaisen, S. K., & Ahmed, Q. W. (2012). Finite element modeling of composite steel-concrete beams with external prestressing. International Journal of Civil & Structural Engineering, 3(1), 101-116.